

# Influence of Pr<sup>3+</sup> ion doped in Infra-red spectroscopy and Elastic properties Co ferrites

<sup>1</sup>Pachpinde AM, <sup>1</sup>Langade MM, <sup>2</sup>Dhale LA, <sup>2</sup>Ganure Keatn A and <sup>2</sup>Lohar KS

<sup>1</sup>Department of Chemistry, Shrikrishna Mahavidhyalaya, Gunjoti, Tq. Omerga, 413613 Maharashtra.

<sup>2</sup>Department of Chemistry, Jwahaar Art, Science and Commerce College, Andur, Tq. Tuljapur, Maharashtra.

\* Corresponding author email: [kslohar@rediffmail.com](mailto:kslohar@rediffmail.com)

## Manuscript Details

Available online on <http://www.irjse.in>  
ISSN: 2322-0015

Editor: Dr. Arvind Chavhan

### Cite this article as:

Pachpinde AM, Langade MM, Dhale LA, Ganure Keatn A and Lohar KS. Influence of Pr<sup>3+</sup> ion doped in Infra-red spectroscopy and Elastic properties Co ferrites, *Int. Res. Journal of Science & Engineering*, 2018; Special Issue A5: 105-110.

© The Author(s). 2018 Open Access

This article is distributed under the terms  
of the Creative Commons Attribution

4.0 International License

(<http://creativecommons.org/licenses/by/4.0/>),  
which permits unrestricted use, distribution, and  
reproduction in any medium, provided you give  
appropriate credit to the original author(s) and the  
source, provide a link to the Creative Commons  
license, and indicate if changes were made.

## ABSTRACT

Pr<sup>3+</sup> doped Pr<sub>x</sub>CoFe<sub>2-x</sub>O<sub>4</sub> (x = 0.0, 0.025, 0.05, 0.075, 0.1) ferrite nanoparticles prepared by using sol-gel auto-combustion method. The prepared samples sintered at 600 °C for 4 hours. Infrared spectra carried out at room temperature in the wavenumber range of 300–800 cm<sup>-1</sup>. The IR spectra show two major absorption bands. High frequency bands 'ν<sub>1</sub>' is assigned to the tetrahedral and low frequency bands 'ν<sub>2</sub>' is assigned to the octahedral sites of complex. Force constant for the tetrahedral and octahedral site was determined by using IR data. The values of Force constant use to calculate the Stiffness constants (C<sub>11</sub> and C<sub>12</sub>). Using the values of stiffness constants; Elastic moduli such as Young's modulus, Rigidity modulus, Poisson's ratio and Debye temperature are calculated.

**Keywords:** Sol-gel method, Ferrites, infra- red spectroscopy, elastic property.

## INTRODUCTION

Ferrites have been the subject of extensive investigation in last few decades due to their wide range of applications such as information storage systems, gas sensors, microwave devices and magnetic recording and electronic industries [1]. The possibility of mixing metals in different compositions makes ferrites very attractive. Spinel ferrites with cubic structure are one of the most attractive materials for magnetic, catalysis,

microelectronic and gas sensing applications [2-5]. Cobalt ferrites have been regarded for high density magnetic recording media because of its moderate saturation magnetization, high coercivity, mechanical hardness and chemical stability [6]. Ferrites samples prepared several methods. Such as Solid state reaction [7], Hydrothermal preparation [8], Micro emulsion method [9], Oxalate Precursors method [10]. Now a day, among these various preparation methods of the ferrite nanoparticles, the Sol-gel auto-combustion method commonly used. The elastic constant is important because of them elucidates the nature of the binding forces in the solid. The elastic modulus represents the mechanical strength fracture toughness and thermal stock resistance [11].  $\text{Pr}_x\text{CoFe}_{2-x}\text{O}_4$  ( $x = 0.0, 0.025, 0.05, 0.075, 0.1$ ) were synthesized by Sol-gel Auto-Combustion method and also examine the effect of  $\text{Pr}^{3+}$  substituted in Co ferrites on the elastic properties.

## METHODOLOGY

Nano crystalline ferrite powders with compositions of  $\text{Pr}_x\text{CoFe}_{2-x}\text{O}_4$  ( $x = 0.0, 0.025, 0.05, 0.075, 0.1$ ) were synthesized by Sol-gel Auto-Combustion technique. The metal nitrates (A.R. grade with 99.8 % purity) Cobalt nitrate. Praseodymium nitrate  $\text{Pr}(\text{NO}_3)_3 \cdot 6\text{H}_2\text{O}$ , Cobalt nitrate  $\text{Co}(\text{NO}_3)_2 \cdot 6(\text{H}_2\text{O})$  Ferric Nitrate ( $\text{Fe}(\text{NO}_3)_3 \cdot 9\text{H}_2\text{O}$ ), and Citric acid ( $\text{C}_6\text{H}_8\text{O}_7 \cdot \text{H}_2\text{O}$ ) were used as starting materials. Reaction was carried out in air atmosphere without protection of inert gases.

The molar ratio of metal nitrates to citric acid was taken as 1:3. The metal nitrates were dissolved together in a minimum amount of double distilled water to get a clear solution. An aqueous solution of citric acid was mixed with metal nitrates solution, then ammonia solution was slowly added to adjust the  $\text{pH} \cong 7$ . The mixed solution was kept on to a hot plate with continuous stirring at  $90^\circ\text{C}$ . During evaporation, the solution became viscous and finally formed a viscous brown gel. When finally all water molecules were removed from the mixture, viscous gel began frothing. After few minutes, the gel automatically ignited and burnt with glowing flints. The decomposition reaction

would not stop before the whole citrate complex was consumed. The auto-combustion was completed within a minute, yielding the brown-coloured ashes termed as a precursor. The as prepared powder then annealed at  $600^\circ\text{C}$  for 4 hrs.

The prepared samples were characterized by X-ray investigations. Part of the powder was X-ray examined by Phillips X-ray diffractometer (Model 3710) using  $\text{Cu-K}_\alpha$  radiation ( $\lambda = 1.5405\text{\AA}$ ). The scanning step was  $0.02^\circ$  and scanning rate was  $2^\circ/\text{min}$ . The infrared spectra of all the samples were recorded at room temperature in the range  $300\text{ cm}^{-1}$  to  $800\text{ cm}^{-1}$ .

## RESULTS AND DISCUSSIONS

### X-ray analysis:

It is obvious from the XRD patterns (Fig. 1) of  $\text{Pr}_x\text{CoFe}_{2-x}\text{O}_4$  that the patterns were indexed and cubic lattice was observed. The results indicate that the material has a well-defined crystalline single phase belonging to the fcc system. The diffraction pattern gave a verification of the presence of spinel crystal structure for each composition of  $\text{Pr}_x\text{CoFe}_{2-x}\text{O}_4$ . Since the XRD patterns of  $\text{PrFeO}_3$  phase for  $x < 0.075$ , we can draw a conclusion that  $\text{Pr}^{3+}$  has entered the lattice of ferrite successfully.[12].

It is observed that the cubic spinel phase coexists with some amount of  $\text{PrFeO}_3$  phase in  $x \geq 0.075$ . As  $\text{CoFe}_2\text{O}_4$  is nearly inverse spinel, this anomaly in the intensity distribution may arise from the following facts: (i) differences in the cation distribution among the [A] and [B] sites in the spinel lattice and; (ii) phase inhomogeneity, in particular presence of ferrite phases with different cation distributions. The ionic radius of  $\text{Pr}^{3+}$  ions is  $1.13\text{\AA}$  which is larger than that of  $\text{Fe}^{3+}$  ( $0.67\text{\AA}$ ), and the amount of  $\text{Fe}^{3+}$  ions substituted by  $\text{Pr}^{3+}$  ions is limited, thus redundant  $\text{Pr}^{3+}$  ions aggregates on the grain boundaries forming  $\text{PrFeO}_3$  phase. As a result, there was a limit for the replacement of  $\text{Fe}^{3+}$  with  $\text{Pr}^{3+}$ , and the maximum was  $x = 0.05$  in our experiment. The values of lattice constant and x-ray density calculated are given by Table.1

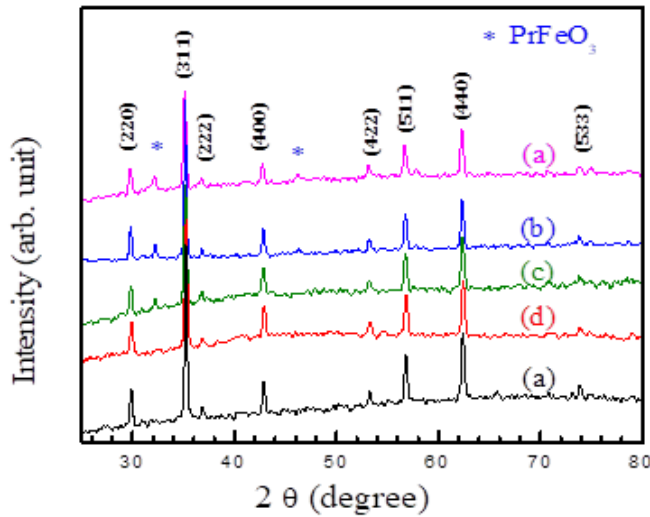


**Fig. 1:** X-Ray diffraction patterns of (a)  $x = 0.0$ , (b)  $x = 0.025$ , (c)  $x = 0.050$ , (d)  $x = 0.075$  and (e)  $x = 0.1$  for  $\text{Pr}_x\text{CoFe}_{2-x}\text{O}_4$

The lattice constant 'a' increases from 8.373- 8.423 Å with increase in  $\text{Pr}^{3+}$  substitution. The ionic radius of  $\text{Pr}^{3+}$  and  $\text{Fe}^{3+}$  ions is 1.13 and 0.67 respectively, therefore, when  $\text{Fe}^{3+}$  was replaced by  $\text{Pr}^{3+}$  the lattice constant should aggrandize as the content of the  $\text{Pr}^{3+}$  increased. The relationship between  $\text{Pr}^{3+}$  substitution and lattice parameter can be explained by Vegard's law [13].

**Infra-red Spectroscopy:**

The obtained IR spectrum in the range 200-800  $\text{cm}^{-1}$  for nanocrystalline  $\text{Pr}_x\text{CoFe}_{2-x}\text{O}_4$  ferrite system is illustrated in Fig. 2. The observed variation in absorption bands for the present investigated system is listed in Table 1. It is observed from Table 1. IR spectrum of the synthesized samples displayed two absorption bands characteristic of the spinel ferrites at 707-757 and 454-477  $\text{cm}^{-1}$ . The higher frequency band ( $\nu_1$ ) was due to stretching vibration of tetrahedral metal oxygen bond and the lower frequency band ( $\nu_2$ ) was due to octahedral metal oxygen bond [13]. The band positions for all the investigated composition are given in Table 1. The change in the lattice constant is responsible for this shift of the center frequencies.

The increase in the unit cell dimensions due to the replacement of  $\text{Fe}^{3+}$  ions by larger ionic radius  $\text{Pr}^{3+}$  ions affects the  $\text{Fe}^{3+}\text{-O}^{2-}$  stretching vibrations and this is a

prominent cause of change in band positions. The change in the frequency of  $\nu_1$  stretching band indicates the preference of  $\text{Pr}^{3+}$  ions to occupy the octahedral sites. The peak intensity of frequency bands slightly changes within increasing  $\text{Pr}^{3+}$  substitution. It is known that the intensity ratio is a function of the change of dipole moment with the inter-nuclear distance ( $d\mu/dr$ ) [14]. This value represents the contribution of the ionic bond Fe-O in the lattice. Furthermore, it is observed from Fig. 5.10 that the normal mode of vibration of tetrahedral cluster ( $\nu_1$ ) is higher than that of octahedral cluster ( $\nu_2$ ), which is attributed to the shorter bond length of tetrahedral cluster and longer bond length of octahedral cluster. Using the analysis of Waldron [13], the force constant  $K_0$  and  $K_t$  were calculated

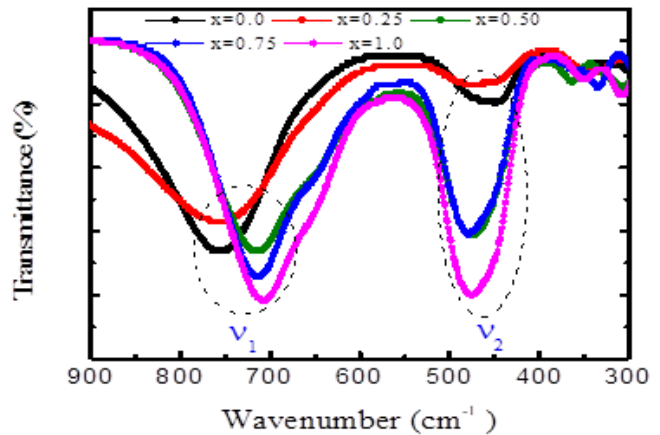


**Fig 2:** Infrared spectra for the series  $\text{Pr}_x\text{CoFe}_{2-x}\text{O}_4$ .

According to Waldron the force constant  $K_t$  and  $K_o$  for respective sites are given by:

$$K_t = 7.62 \times M_1 \times \nu_1^2 \times 10^{-3} \tag{1}$$

$$K_o = 10.62 \times \frac{M_2}{2} \times \nu_2^2 \times 10^{-3} \tag{2}$$

Where,  $K_o$  = force constant on octahedral site,  $K_t$  = force constant on tetrahedral site,  $M_1$  = Molecular weight of tetrahedral site,  $M_2$  = Molecular weight of octahedral site,  $\nu_1$  = Corresponding center frequency on tetrahedral site,  $\nu_2$  = Corresponding center frequency on octahedral site. The values of force are summarized in Table 1. The force constant  $K_t$  decreasing with the increasing  $\text{Pr}^{3+}$  content whereas  $K_o$  increases with the increasing in  $\text{Pr}^{3+}$ . This variation can be related with the difference in ionic radii

of Fe<sup>3+</sup> and Pr<sup>3+</sup> ions and their occupancy at A and B sites. Analysis of IR spectra with crystallographic knowledge helps us to determine the Debye temperature and elastic properties. The Debye temperature ( $\theta_D$ ) of all samples was calculated using the wave number of IR bands. [14].

$$\theta_D = hCv_{av}/k$$

Where,  $h = h/2\pi$ ,  $k$  is Boltzman constant,  $C$  is velocity of light ( $C = 3 \times 10^{10}$  cm/s) and  $v_{av}$  is average wave number of bands. Variation of Debye temperature with Pr content is shown in Fig. 3

### Elastic properties:

The elastic properties were determined using infrared spectroscopy [15-16] These elastic moduli were calculated using the values of lattice constant 'a', X-ray density 'd<sub>x</sub>', pore fraction 'f' and force constant 'K'. Values of lattice constant, X-ray density and pore fraction are listed in Table 1. The average force constant (K) was calculated using the following relation:

$$k = kt + ko/2 \quad (4)$$

The bulk modulus of term stiffness constant  $C_{11}$  was calculated using relation [17] Stiffness constant

$$C_{11} = \frac{K}{a} \quad (5)$$

Where  $K$  is average force constant and  $a$  is lattice constant.

$$\text{Stiffness constant } (C_{12}) = \frac{\sigma \times C_{11}}{(1 - \sigma)} \quad (6)$$

where  $\sigma$  is Poisson ratio and 'a' is the lattice constant. The Poisson ratio is function of pore fraction ( $\sigma = 0.324 \times 1 - 1.043f$ ). Values of Poisson ratio are presented in Table 2. The Poisson ratio is ranges in between 0.276 and 0.266, these values are lie in the range of -1 to 0.5, which is in conformity with the theory of isotropic elasticity. [16]

Variation of stiffness constants ( $C_{11}$  and  $C_{12}$ ) as a function of Pr<sup>3+</sup> content is shown in table.2. It is observed from Table 2; both the stiffness constant was decreases with increase in Pr<sup>3+</sup> substitution. The values of

Poisson's ratio were calculated using the relation discussed elsewhere [17] and the values are presented in table 2. Use of stiffness constant are affected by two factors; i.e. the tightness of bonding between the atoms and force constant. In present system bonds between Fe<sup>3+</sup> and Pr<sup>3+</sup> atoms is residual bond and due to this stiffness constant are decreases with increasing Al content. These two stiffness constants are further used to calculate the various elastic constants such as; Young's modulus (E), bulk modulus (K) and modulus of rigidity (G) [14]. The other elastic moduli for cubic structure are calculated using following relation [18].

$$\text{Rigidity modulus } (G) = \frac{E}{2(\sigma + 1)} \quad (7)$$

The rigidity modulus (G) is calculated using the relation 3 and the variation are presented in Table 2. It can be observed from Table 2 the values of rigidity modulus increased with Pr<sup>3+</sup> substitution. B, G, E decrease with increase in both Pr<sup>3+</sup> it indicates that deformation of the solid is easy and the solid has less tendency to spring back to its equilibrium position. the Young's modulus, Bulk modulus and modulus of rigidity decreases with the increasing Pr<sup>3+</sup> content. The decreases in elastic moduli may be due to the interatomic binding between various atoms in the spinel lattice. [15]. The inter-atomic bonding between the various atoms weakens continuously with the addition of Pr<sup>3+</sup> content and therefore elastic moduli decreases with the increasing Pr<sup>3+</sup> content. In Fe<sup>3+</sup>-Pr<sup>3+</sup> ferrite repulsion between electrons may be increased with the increasing Pr<sup>3+</sup> content. [14]

The longitudinal elastic wave velocity ( $V_L$ ) and transverse (Shear) wave velocity ( $V_s$ ) was calculated using following equations,

$$\text{Longitudinal velocity } V_L = \left( \frac{C_{11}}{\rho} \right)^{1/2} \quad (8)$$

$$\text{Transverse (Shear) velocity } V_s = \left( \frac{G}{\rho} \right)^{1/2} \quad (9)$$

Where  $G$  is rigidity modulus with correct zero pore fraction. The values of  $V_L$  and  $V_s$  used to calculate mean

wave velocity ( $V_m$ ) which used to calculate Debye temperature was calculated using formula

$$\theta_E = \frac{h}{k} \left[ \frac{3\rho q N_A}{4\pi M} \right]^{1/3} \times V_m \quad (10)$$

Where h is planks constant, k is Boltzmann's constant, M is molecular weight, q is number if atom in the unit formula and  $V_m$  mean wave velocity

$$\frac{3}{V_m^3} = \frac{1}{V_l^3} + \frac{2}{V_s^3} \quad (11)$$

The values of longitudinal wave, shearing wave and mean wave velocity are calculated using relation 4, 5 and 7 respectively. It is observed from Table 3, the longitudinal elastic wave velocity is decreases whereas transverse (Shear) wave velocity increased with  $Pr^{3+}$  substitution. The values of wave velocities are similar to other ferrites those obtained from UPT method [20]. The variation of Debye temperature ( $\theta_E$ ) is given Table 3. The Debye temperature increased with  $Pr^{3+}$  substitution. It suggested that lattice vibrations are hindered due to  $Pr^{3+}$  substitution. This may be due to the fact that strength of interatomic bonding increases with concentration (x and y) as supported by our results on the variation of elastic moduli.

**Table 1:** Lattice constant (a), X-ray Density (dx), Band Position ( $v_1$  and  $v_2$ ), force constant ( $K_o$  and  $K_t$ ) of  $Pr_xCoFe_{2-x}O_4$

Comp. x	'a' (Å)	'd <sub>x</sub> ' (g/cm <sup>3</sup> )	Band position		Force constant	
			$v_1$ (cm <sup>-1</sup> )	$v_2$ (cm <sup>-1</sup> )	$K_o \times 10^5$ (dyne/cm)	$K_t \times 10^5$ (dyne/cm)
0.0	8.3732	5.309	757	454	1.293	2.441
0.025	8.3761	5.352	754	461	1.272	2.399
0.05	8.3835	5.386	718	471	1.266	2.147
0.075	8.3984	5.405	713	477	1.227	2.118
0.1	8.4234	5.404	707	475	1.133	2.121

**Table 2:** Mean force constant (K), pore fraction Stiffness constant ( $C_{11}$  and  $C_{12}$ ), of  $Pr_xCoFe_{2-x}O_4$ .

Comp. x	Mean Force constant ( $K_t+K_o$ )	Pore Fraction	Passion's ratio $\sigma$	$C_{11}$	$C_{12}$
0.0	1.8671	0.142	0.276	222.98	85.01
0.025	1.8356	0.148	0.274	219.15	82.70
0.05	1.7068	0.154	0.272	203.59	76.05
0.075	1.6725	0.163	0.269	199.14	73.25
0.1	1.6268	0.172	0.266	193.13	69.95

**Table 3:** Rigidity modulus (G)Young modulus(Y), Bulk Modulus (B), longitudinal elastic wave velocity ( $V_L$ ) and transverse (Shear) wave velocity ( $V_s$ ), mean wave velocity ( $V_m$ ), Debye temperature ( $\Theta_E$ ) of  $Pr_xCoFe_{2-x}O_4$ .

Comp. x	G	Y	B	$V_L$	$V_s$	$V_m$	$\Theta_E$
0.0	91.391	176.05	131.00	6480.77	3280.30	3641.74	498
0.025	91.880	173.83	128.19	6399.03	3288.72	3651.09	500
0.05	87.350	162.23	118.56	6148.18	3277.82	3638.99	499
0.075	88.532	159.75	115.22	6069.94	3280.95	3642.46	501
0.1	89.068	155.94	111.01	5978.18	3295.66	3658.79	503

## CONCLUSION

The Pr<sup>3+</sup> substituted Pr<sub>x</sub>CoFe<sub>2-x</sub>O<sub>4</sub> (x=0.0, 0.025, 0.05, 0.075, 0.1) ferrite nanoparticles were prepared by using sol-gel auto-combustion method. The Elastic properties such as elastic wave velocity, elastic constant and Debye temperature calculated using XRD and IR data. The elastic constants decreased with the increasing in Pr<sup>3+</sup> content.

## REFERENCES

- Mohammed KA, Al-Rawas AD, Gismelseed AM, Sellai A, Widatallah HM, Yousif A, Elzain ME, M Shongwe. *Physica B*; 407,2012, 795.
- Li. Y, Li Q, Wen M, Jhang Y, Jhai Y, Xie Z, Xu F, Wei S. *J. Electron Spectrom. Relat. Phenom*, 160, 2007,1.
- Lee PY, Ishizaka K, Shematsu H, Jijang W, Yatsui K. *J. Nanopart. Res.*, 8, 2006, 29.
- Zhihao Y, Lide Z. *Mater. Res. Bull.*, 33,1998, 1587.
- Dube GR, Darshane VS. *J. Mol. Catal.*, 79, 1993, 285.
- Singhal S et al. *Journal of Magnetism and Magnetic Materials*, 306, 2006, 233-240
- Kaunda K, Mishra S. *Bull. Mater. Sci.*, 31,2008,507-510.
- Lucke R, Schlegel E and Strienitz R. *J. Phys. IV FRANCE*, 7, 1997, C1-63.
- Lodhi Maria Yousaf, mahmood Khalid, Mahmood Azhar, malik Huma, Warsi Muhammad Farooq, Imran shakir, M.Asghar, Khan, Muhmaad Azhar, *Current Applied Physics*, 14, 2014, 716.
- Panda RN, Shih JC, Chin TS. *Journal of Magnetism and Magnetic Materials*, 257, 2003, 79-86.
- Modi KB, Trivedi UN, Shrama PU, Lkakhani VK, Chhantbar MC, Joshi HH. *Journal of pure and applied physics*, 44, 2006, 165-168.
- Pachpinde AM, Langade MM, Patange SM, Shirsath Sagar E. *Chemical Physics*, 429, 2014, 20-26.
- Vegard L. *Z. Phys.*, 5, 1921, 17-26.
- Waldron RD. *Phys. Rev.*, 99, 1955, 1727.
- Shirsath Sagar E, Patange SM, Kadam RH, Mane ML, Jadhav KM. *J. Mole. Structure*, 1024, 2012, 77-83.
- Modi KB, Gajera JD, Pandya MP, Vora HG, Joshi HH, *Pramana, Journal of physics.*, 62, 2004, , 1173-1180.
- Belavi PB, Naik LR, Chavan GN, ISSN-Science, 41, 2015, 2.
- Modi KB, Chhantbar MC, Joshi HH. *Ceramic. Inter.*, 32, 2005,111.
- Patil VG, Shrisath Sagar E, More SD, Shukla SJ, Jadhav KMJ. *Alloys Compd.*, 488, 2009, 199-203
- Bhatu SS, Lakhani VK, Tanna AR, Varsoya NH, Buch JU, Sharma PU, Trivedi UN, Joshi HH, Modi KB. *Ind. J. Pure Appl. Phys.*, 45, 45,596.
- Mazen SA, Elmosalami TA. *ISRN Condensed Matter Physics*, 2011, 9.

© 2018 | Published by IRJSE

### Submit your manuscript to a IRJSE journal and benefit from:

- ✓ Convenient online submission
- ✓ Rigorous peer review
- ✓ Immediate publication on acceptance
- ✓ Open access: articles freely available online
- ✓ High visibility within the field

Email your next manuscript to IRJSE  
: editorirjse@gmail.com